

FULL PAPER

Active site elucidation and optimization in Pt co-catalysts for photocatalytic hydrogen production over titania

Zhi Jiang,^{*[a]} Mark A. Isaacs,^[b] ZhengWen Huang,^[a] Wenfeng Shangguan,^[a] Yifeng Deng,^[c] and Adam F. Lee^{*[b]}

Abstract: Platinum co-catalysts play a critical role in promoting the photocatalytic performance of inorganic semiconductors, yet despite intensive investigation, the active platinum species responsible remains controversial. Here the physicochemical properties of Pt nanoparticles introduced into anatase titania through three different synthetic protocols are investigated by porosimetry, XRD, XPS and XAS and correlated with their corresponding activity for aqueous photocatalytic hydrogen production. Conventional wet impregnation produces small but highly oxidized platinum nanoparticles due to the classical strong metal-support interaction with titania during high temperature processing. Photodeposition yields predominantly metallic but large and inhomogeneous (1.5–7.5 nm) Pt nanoparticles. In contrast, a modified in-situ polyol route affords metallic and highly dispersed (<2 nm) nanoparticles with minimal PtO_x. Photocatalytic H₂ evolution is directly proportional to the surface concentration of Pt metal, conclusively demonstrating metallic platinum as the active co-catalyst, and offering a simple parameter to quantitatively predict the photocatalytic performance of Pt/TiO₂ in H₂ production. The modified in-situ polyol synthesis is optimal for co-catalyst formation, delivering rate enhancements of 25–80 % compared to the other syntheses.

Introduction

Light-driven water splitting for the direct production of molecular hydrogen is one of the most promising routes to solar energy conversion and storage [1]. Inorganic semiconductors are promising materials to effect this photochemical conversion, whose efficiency mainly depends on successful charge creation, separation and migration within the semiconductor^[2], as well as the kinetics of the subsequent bond breaking and making surface reactions, which are in turn strongly influenced by the presence and nature of co-catalysts on the semiconductor surface [3]. The role of the latter is often neglected, hindering the rational design of co-catalysts and their associated impact on photocatalytic performance in water splitting.

Transition metal nanoparticles represent the most common co-catalysts employed to promote semiconductor photocatalysts, notably Pt, however contradictory findings are reported regarding the oxidation state of Pt co-catalysts in water splitting [4]. For example, Li et al reported optimal photocatalytic hydrogen production over PtO^[5], whereas Xing and co-workers propose electron-deficient (atomically-dispersed) Pt^{δ+} species are superior to metal clusters [6]. In contrast, our preliminary studies on photodeposited Pt/TiO₂ indicate an important role for metallic platinum [7]. This confusion stems in part from the diverse literature syntheses employed to introduce platinum nanoparticles, and attendant variations in Pt concentration (loading), size, oxidation state and morphology. To date, the impact of different synthetic approaches on the physicochemical properties of Pt nanoparticle co-catalysts incorporated into titania photocatalysts (the most popular materials for diverse photocatalytic transformations despite their poor spectral response and quantum efficiencies) has not been systematically studied. Hence there is a dearth of efforts to develop simple structural predictors of photocatalytic performance. Recently, an in-situ polyol method proved advantageous in creating such hybrid photocatalysts [8], but remained unsuitable for generating particle sizes <2.5 nm from the most common, and low cost, H₂PtCl₆ precursor which yielded 6–7 nm diameter particles. Photodeposition (PD) is another method to load metal co-catalysts on a semiconductor photocatalyst. We recently employed PD to produce highly dispersed metallic Pt nanoparticles over titania through varying the methanol concentration during photoirradiation; photocatalytic hydrogen production from water was related to the surface density of Pt metal. However, in the absence of methanol, PD produced predominantly electron-deficient platinum which was unstable with respect to sintering during subsequent photocatalytic hydrogen production. Wetness impregnation is the most general method to load metal nanoparticles over oxide supports [4a–c], but offers poor control over the resulting particle morphology.

Anatase is known to be inactive for splitting pure water (i.e. in the absence of a hole scavenger) into hydrogen and oxygen in the nominal 2:1 stoichiometry [9], hence here we compare the impact of the preceding three routes on the physicochemical properties of Pt co-catalysts on photocatalytic water splitting over anatase in the presence of a sacrificial hole acceptor. A pH controlled in-situ polyol synthesis employing a H₂PtCl₆ precursor efforts proved an effective route to prepare uniform, highly dispersed Pt metal nanoparticles over titania. Highly dispersed, but electron deficient, Pt nanoparticles were accessible over anatase through tuning wet impregnation. Metallic Pt is shown to be the active co-catalyst for H₂ evolution from water splitting over anatase.

[a] Dr.Z. Jiang, Prof. Dr. W.Shangguan
Research Center for Combustion and Environment Technology
Shanghai Jiao Tong University
Shanghai, China
E-mail: zhijiang@sjtu.edu.cn

[b] Dr. M.A. Isaacs, Prof. Dr. A.F.Lee
European Bioenergy Research Institute
Aston University
Birmingham, UK
E-mail: a.f.lee@aston.ac.uk

[c] Mr. Y.Deng
Pinghe School
Shanghai, China

Results and Discussion

The physicochemical properties of the four families of 1wt% Pt/TiO₂ catalysts were first characterized by a range of bulk and surface sensitive analytical techniques. **Figure 1** compares powder XRD patterns of these materials, which all exhibited reflections characteristic of anatase crystallites (JCPDS 21-1272) whose relative intensities and line shapes were essentially identical, indicating a common morphology and volume averaged particle diameter of ~14 nm (calculated from the Scherrer equation as shown in **Table 1**), presumably as a consequence of their similar thermal processing history. In contrast, the different synthetic methods resulted in significant variations in the intensity of fcc platinum metal reflections (JCPDS65-2868), with the principal 39.8 ° reflection only observed for PD.

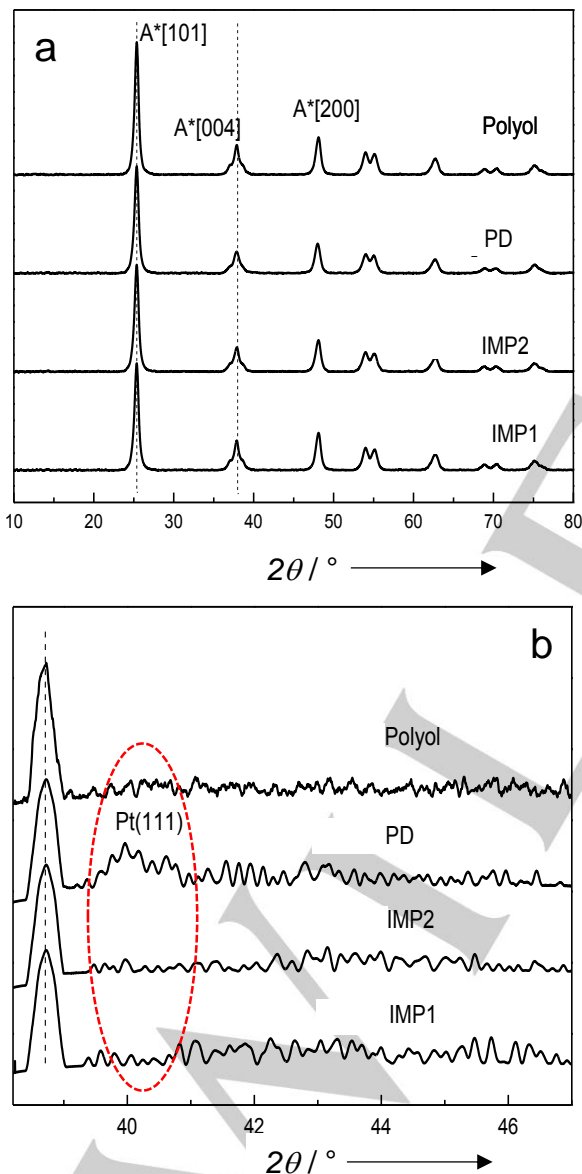


Figure 1. (a-b) Powder XRD pattern of 1 wt% Pt/TiO₂ catalysts as a function of synthetic route, highlighting fcc platinum reflection. A* = anatase phase titania.

Figure 2 compares the DRUV spectra of the as-prepared Pt/TiO₂ samples. All materials exhibited similar optical properties, with strong absorption edges at about 390 nm due to the band gap absorption of pure anatase TiO₂. Nitrogen porosimetry of the 1 wt% Pt/TiO₂ samples confirmed they possessed similar textural properties, with the four synthetic routes affording a common surface area of approximately 110 m².g⁻¹ (**Table 1**). Elemental analysis also confirmed that the actual and nominal loadings of all four 1 wt% Pt/TiO₂ were essentially identical; the absence of metallic Pt diffraction features for the wet impregnation and in-situ polyol syntheses is thus indicative of the presence of highly dispersed, or oxidic, Pt species over the anatase support. It is important to note that any differences between the catalytic performances of these materials (described subsequently) cannot therefore be attributed to variations in either titania phase/morphology, or platinum loading.

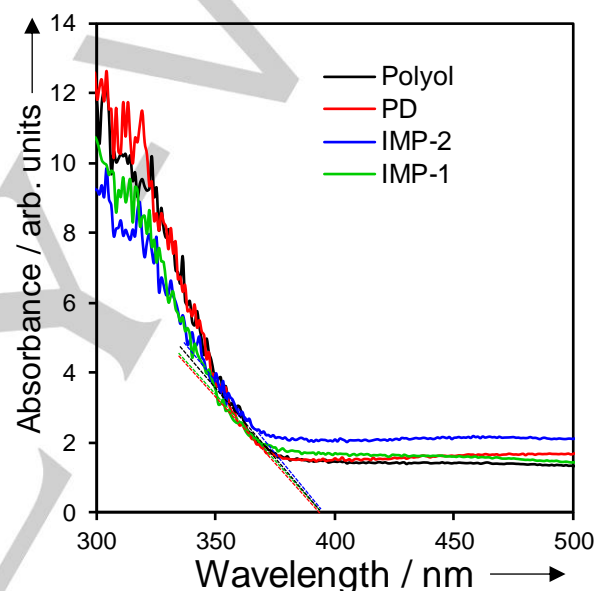


Figure 2. DRUV spectra of 1 wt% Pt/TiO₂ catalysts as a function of synthetic route.

Table 1. Structural properties of 1 wt% Pt/TiO₂ catalysts

Sample	Pt loading ^[a] / wt%	BET area ^[b] / m ² .g ⁻¹	surface area ^[c] / nm	Anatase size ^[c] / nm	particle size ^[c] / nm
Pt/TiO ₂ -Polyol	1.09	107		13.4	
Pt/TiO ₂ -PD	1.06	106		13.2	
Pt/TiO ₂ -IMP-2	1.06	108		14.0	
Pt/TiO ₂ -IMP-1	1.08	109		13.9	

^[a]ICP-AES; ^[b]N2 porosimetry; ^[c]XRD.

Platinum particle morphologies for the 1 wt% Pt/TiO₂ materials were investigated by HAADF-STEM (**Figure 3**). Both wet impregnation and the in-situ polyol syntheses resulted in

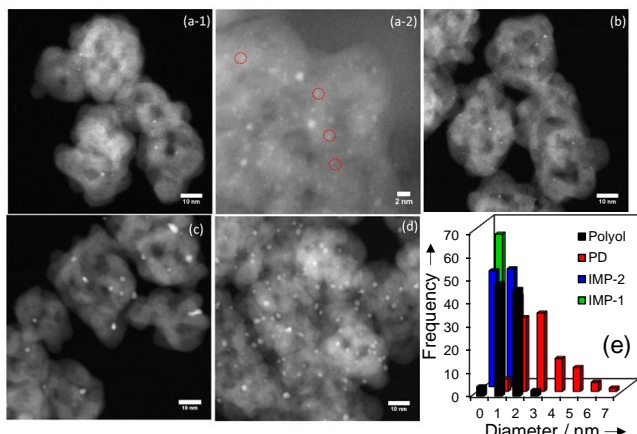


Figure 3. HAADF-STEM images of 1 wt% Pt/TiO₂ catalysts as a function of synthetic route: (a-1 and a-2) IMP-1; (b) IMP-2; (c) PD; (d) in-situ polyol; and (e) corresponding Pt particle size distributions.

small Pt nanoparticles below 2 nm, of which the latter were almost monodispersed at 2±0.25 nm (**Figure 3d-e**). Pt nanocrystals produced in the present in-situ polyol method (performed at pH 9) differ from those previously reported without pH regulation [^{8a}] in which the same H₂PtCl₆ precursor produced far larger 7 nm particles. This suggests that pH plays strongly influences the reduction kinetics and hence size control; indeed basic conditions are known to accelerate ethylene glycol dehydration to acetaldehyde [¹⁰], the latter being a potent reductant of metal salts which likely promotes metal nanoparticle nucleation versus growth. In contrast, PD resulted in a broad distribution of Pt nanoparticle sizes, spanning 1.5–7.5 nm, and irregular shapes (**Figure 3c**). Lattice fringes of the anatase and metallic Pt components of the 1 wt% Pt/TiO₂ samples were also visualised by bright-field TEM (**Figure 4**). **Figure 4** also evidences a close interaction of Pt with the titania surface, notably for 1 wt% Pt/TiO₂-IMP1 wherein the oxide support appears to have partially encapsulated a platinum nanoparticle characteristic of a classical strong metal-support interaction. Wet impregnation of pre-calcined anatase (1 wt% Pt/TiO₂-IMP2) resulted in a slightly broader and larger mean particle size relative to direct impregnation of the as-prepared anatase (1 wt% Pt/TiO₂-IMP2) which may reflect a smaller number of vacancies in the former which act as surface nucleation sites for Pt species.

Surface compositions and platinum oxidation states were determined by XPS (detailed fitted parameters provided in **Table S1**). **Figure 5** shows the resulting Pt 4f XP spectra of the 1 wt% Pt/TiO₂ samples which exhibit the expected spin-orbit split doublets separated by ~3.3 eV. All spectra could be fitted with either a 4f_{7/2} metallic component at 70 eV binding energy, a Pt⁴⁺ component at 73.4 eV attributable to PtO₂, or an intermediate state 71.2 eV which has been previously assigned to Pt-O-Ti species [¹¹]. Only metallic Pt was observed for the 1 wt% Pt/TiO₂-Polyol (**Figure 6**), which also exhibited the highest total surface Pt content (0.29 atom%) and hence dispersion of platinum over the anatase support. This finding is consistent with XRD and TEM, and confirms that the modified in-situ polyol synthesis was most

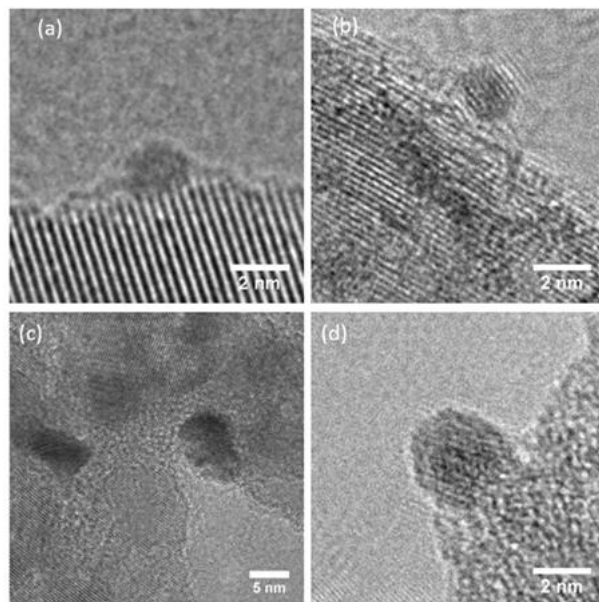


Figure 4. Representative bright-field HRTEM images of 1 wt% Pt/TiO₂ as a function of synthetic route: (a) IMP-1; (b) IMP-2; (c) PD; (d) in-situ polyol

effective in creating small (almost entirely) metallic Pt nanoparticles. PD also favoured metallic nanoparticles, with only ~24 % of surface platinum in oxidised form, but with a significantly lower surface Pt content (0.17 atom%) consistent with larger particles. In contrast, both wet impregnation syntheses favoured heavily oxidised platinum (87–96 % PtO₂/Pt-O-Ti), almost entirely due to the formation of interfacial Pt-O-Ti species arising from the high temperature calcination steps and subsequent incomplete reduction (the latter is known to promote a strong Ti–O–Pt interaction [¹²]). Wet impregnation also yielded the lowest total surface Pt:Ti atomic ratios, indicating the poorest Pt dispersion.

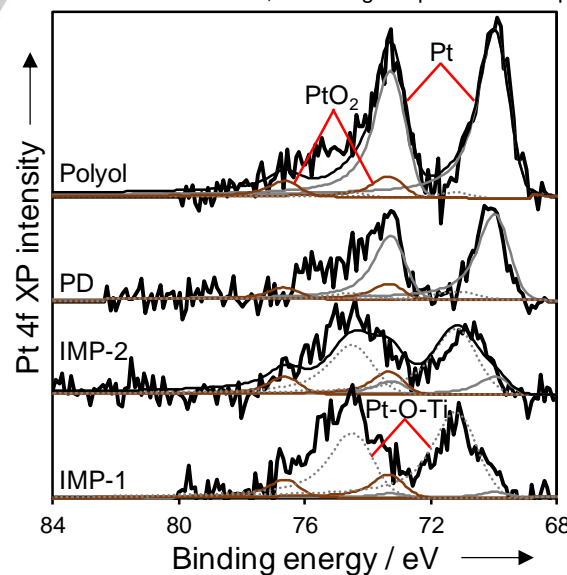


Figure 5. Fitted Pt 4f XP spectra of 1 wt% Pt/TiO₂ catalysts as a function of synthetic route.

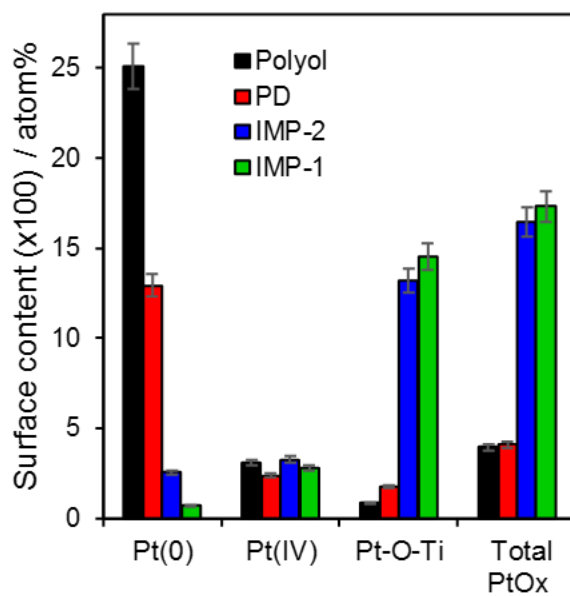


Figure 6. Evolution of surface platinum species of 1 wt% Pt/TiO₂ catalysts as a function of synthetic route.

The mean oxidation state of platinum within the 1 wt% Pt/TiO₂ samples was also explored by XAS. Pt L_{III}-edge XANES in **Figure 7a** confirm that both the in-situ polyol and PD routes yielded spectra almost identical to bulk Pt metal, whereas both wet impregnation routes resulted in spectra with features characteristic of PtO₂, in excellent agreement with XPS. Corresponding radial distribution functions (**Figure 7b**) reveal a strong Pt-Pt nearest neighbor scattering around 2.78 Å for both in-situ polyol and PD samples, confirming the formation of metallic nanoparticles [¹³]; the weaker intensity of this feature for the in-situ polyol sample suggests that it comprises smaller particles, consistent with XRD, TEM and XPS. Preparation by wet impregnation resulted in a strong Pt-O scatterer around 1.95 Å and weak Pt-Pt feature, consistent with partially oxidized Pt metal nanoparticles arising from the calcination step and/or strong interaction with the anatase support.

Figure 8 presents the corresponding photocatalytic activity of the 1 wt% Pt/TiO₂ materials, which exhibit a strong sensitivity on the preparative route. H₂ evolution was linear with reaction time, evidencing negligible deactivation, in all cases. Activity decreased in the order Pt/TiO₂-Polyol > Pt/TiO₂-PD > Pt/TiO₂-IMP-2 > Pt/TiO₂-IMP-1, precisely mirroring the proportion of surface Pt metal from XPS and evidencing a direct correlation between the platinum oxidation state and degree of titania promotion. The 1 wt% Pt/TiO₂-Polyol catalysts evolved 82 % and 51 % more hydrogen than equivalent Pt/TiO₂-IMP1 and Pt/TiO₂-IMP2 catalysts. Note that identical trends were observed for 0.5 and 2 wt% Pt/TiO₂ catalysts (**Figure S1**), highlighting the general superiority of the in-situ polyol synthesis which still offered highly dispersed (2 nm) particles for the 2 wt% loading (**Figure S2**). The importance of metallic Pt as a co-catalyst most likely arises from either improved charge separation (e.g. acting as electron trap centers) or providing surface sites for hydrogen recombination [^{3e}].

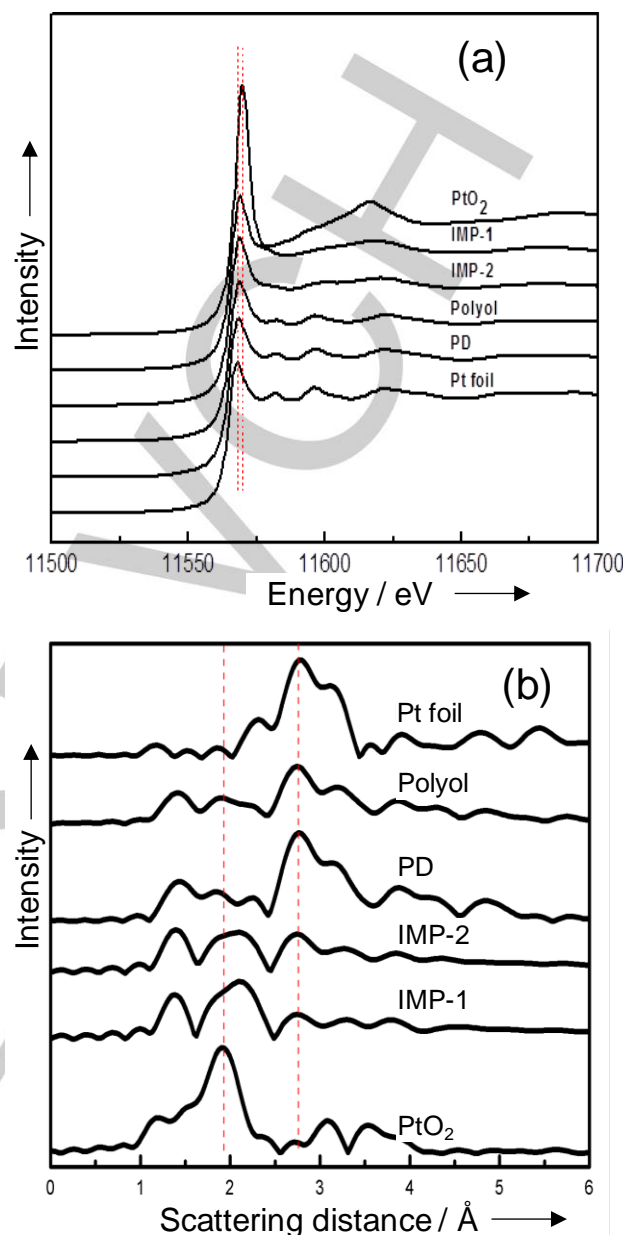


Figure 7. Pt L_{III}-edge (a) normalized fluorescence XANES spectra and (b) corresponding radial distribution functions of 1 wt% Pt/TiO₂ catalysts as a function of synthetic route. Pt foil and oxide references shown for comparison.

The preceding observations are consistent with our previous study using PD to introduce Pt co-catalyst into P25 titania, [⁷] where, in the absence of methanol during the catalyst synthesis, a high density of small, oxidic Pt nanoparticles were formed which exhibited poor subsequent activity for aqueous photocatalytic hydrogen production. Such oxidic nanoparticles were also unstable with respect to in-situ reduction and sintering to form large and inhomogeneous Pt metal nanoparticles. Methanol introduction during the PD step in the present work

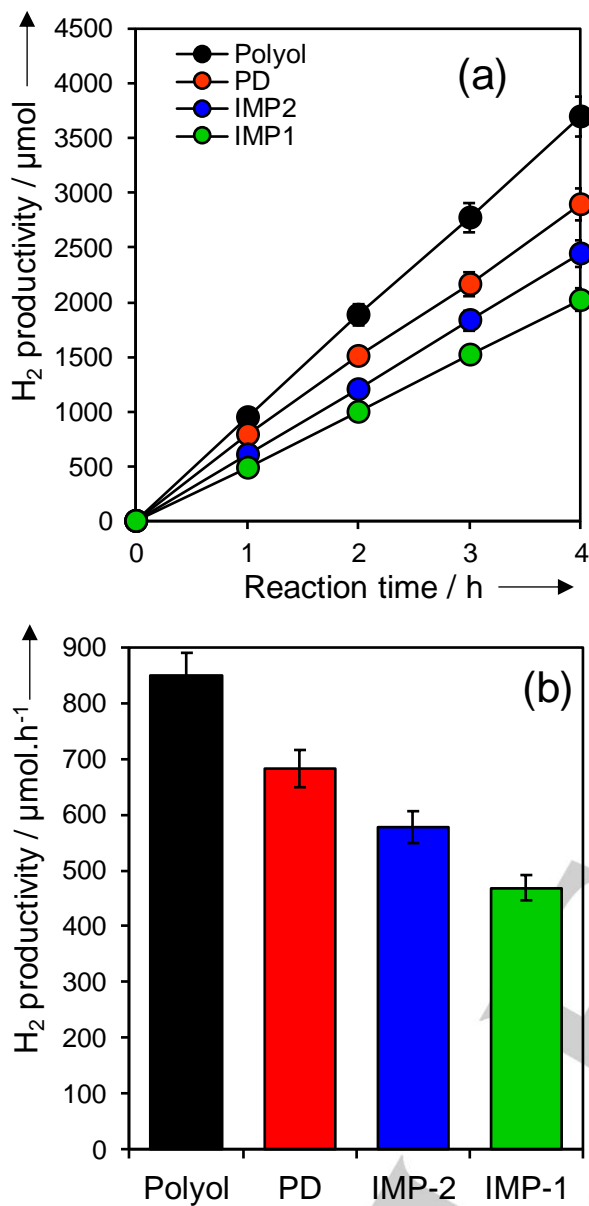


Figure 8. (a) Photocatalytic hydrogen reaction profile and (b) H₂ productivity of 1 wt% Pt/TiO₂ catalysts as a function of synthetic route. Reaction conditions: 50 mg catalyst, 80 ml water and 20 ml methanol.

circumvents these issues. We note that despite the high temperature reduction (400 °C) step employed therein, neither of the two wet impregnation routes in this work were as effective as liquid phase chemical reductions in producing metallic Pt, presumably due to SMSI phenomena which stabilize (or partially encapsulate) oxido platinum. The principal factor influencing the performance of nanoparticulate Pt co-catalysts in promoting photocatalytic H₂ production over anatase is the interfacial concentration of metallic Pt (**Figure 9 a**). Note that pure anatase produced only 55 μmol/h of hydrogen, hence the significant y-axis

intercept (of ~300 μmol/h of hydrogen in terms of surface Pt⁰:Ti atomic ratio, **Fig. S3**) indicates there must be a minimum

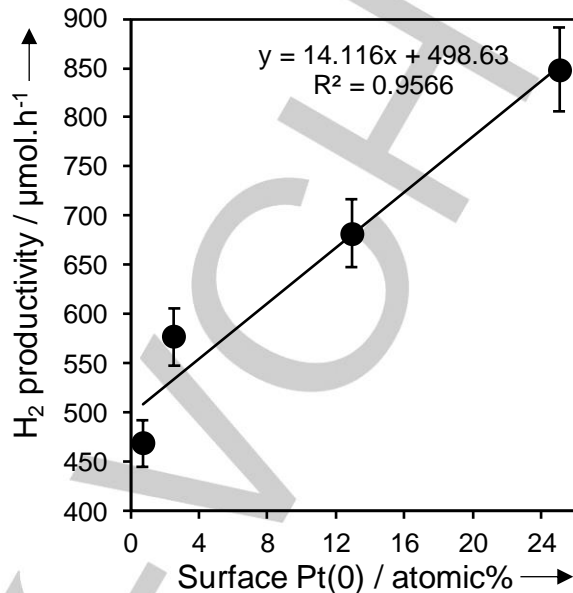


Figure 9. Linear relationship between surface Pt metal concentration and photocatalytic H₂ productivity over 1 wt% Pt/TiO₂. Reaction conditions: 50 mg catalyst, 80 ml water and 20 ml methanol.

ensemble of Pt atoms below which water splitting cannot be sustained, possibly due to both geometric and electronic factors.

Conclusions

The impact of wet chemical synthetic route on the physicochemical properties of platinum co-catalysts introduced by post-modification of a hydrothermally prepared anatase titania was investigated by bulk and surface analysis. Wet impregnation of as-prepared or pre-calcined anatase by chloroplatinic acid favored the formation of highly oxidized platinum nanoparticles, likely due to a strong-metal support interaction that stabilized interfacial Pt-O-Ti species. In contrast, photodeposition and an in-situ polyol synthesis performed under basic conditions both yield metallic Pt, with the in-situ polyol method particularly effective at forming highly dispersed (<2 nm) nanoparticles over anatase. Co-catalyst introduction by any route had negligible impact on the phase or morphology of the anatase support. Subsequent photocatalytic water splitting under UV-Vis irradiation revealed a direct correlation between the surface Pt metal concentration and evolved H₂ productivity, identifying metallic platinum as the active co-catalyst. The modified in-situ polyol route to Pt co-catalyst incorporation offers significant rate enhancements (25–80 %) relative to other conventional routes, and unlocks strategies to optimize other photocatalytic reactions such as CO₂ reduction which employ platinum co-catalysts.

Experimental Section

Anatase synthesis

Anatase titania was prepared by a hydrothermal route as follows. 130 ml titanium(IV) sulfate (Sinoreagent) aqueous solution (0.625M) was placed in a 250 mL Teflon-lined stainless steel autoclave and heated to 130 °C for 8 h. After cooling the resulting suspension was filtered, washed with water and (ethanol) until the filtrate was pH 7, and dried at 80 °C overnight to yield a white powder. Pt/TiO₂ was prepared by four different procedures using the preceding titania with identical 0.5, 1 and 2 wt% Pt loadings, however a detailed physicochemical characterization was only undertaken on the 1 wt% materials. Similar thermal processing treatments were employed for each synthetic route to minimize perturbation of the anatase support.

Wet impregnation

Two series of Pt/TiO₂ catalysts were prepared by wet impregnation from H₂PtCl₆. In the first, 1 g TiO₂ was mixed with the desired concentration of aqueous chloroplatinic acid (H₂PtCl₆, Sinoreagent), subject to 30 min ultrasonication with stirring, and then evaporated to dryness under stirring at 80 °C. The resulting powders were subsequently dried at 110 °C for 12 h and then calcined at 400 °C (ramp rate 2.5 °C/min) in air for 8 h, and finally reduced in flowing hydrogen at 400 °C (ramp rate 2.5 °C/min) for 1 h. These are denoted Pt/TiO₂-IMP-1. The second series were prepared similarly, but employing TiO₂ pre-calcined at 400 °C (ramp rate 2.5 °C/min) for 4 h prior to impregnation with H₂PtCl₆, and with a decreased subsequent calcination time of only 4 h to ensure the titania experienced a total calcination time of 8 h akin to the first series. The second series is denoted Pt/TiO₂-IMP-2.

Photodeposition

PD was conducted within a Pyrex topped reaction cell. The TiO₂ was pre-calcined in air at 400 °C for 8 h (ramp rate 2.5 °C/min) and reduced in hydrogen at 400 °C for 1 hour (heating rate 2.5 °C/min). 1 g of the pre-calcined TiO₂ was subsequently suspended in 80 ml water and 20 ml methanol at 25 °C to which an appropriate amount of H₂PtCl₆ was added, subject to 30 min ultrasonication with stirring, and the reaction vessel subsequently evacuated prior to irradiation with a 300 W Xe lamp for 1 h. The photodeposited powders were filtered and washed with water prior to in vacuo drying at 80 °C for 12 h. These catalysts are denoted Pt/TiO₂-PD.

In-situ polyol

An in-situ polyol method was adapted from our recent work [8a], in which the pH was changed to 9.0 by 2 M NaOH solution addition. In a typical procedure, the appropriate quantity of H₂PtCl₆, 0.1735 g of tetramethylammonium bromide (Aldrich), 0.1665 g of polyvinylpyrrolidone (Aldrich, 29,000 MW) were added to 1 g of TiO₂ and 30 mL of ethylene glycol in a 100 mL round-bottomed flask at 60 °C and subject to 30 min ultrasonication with stirring. The mixture was then purged with Ar and rapidly heated to 180 °C in an oil bath and held at temperature for 25 min under magnetic stirring to yield a dark brown solution. After cooling to room temperature, the solution was centrifuged at 3000 rpm for 5 min, and a dark blue powder collected by discarding the colorless supernatant. The powder was then washed three times by precipitation/dissolution (re-dispersed in 10 mL of ethanol and then precipitated by adding 40 mL of hexane). 0.5 g of the resulting powders was dispersed in 100 mL H₂O and irradiated with a 300 W Xe lamp for 6 h under bubbling air [8b]. This treatment effectively removes organic ligands from the surface of Pt/TiO₂ without perturbing the physicochemical properties of the

underlying as-synthesised catalyst [8b]. The final powders were filtered and washed with water prior to in vacuo drying at 80 °C for 12 h.

Characterization

Elemental analysis of as-prepared Pt/TiO₂ samples were examined by inductively coupled plasma atomic emission spectroscopy (ICP-AES, iCAP 6000 Radial, Thermo). Crystallinity was measured by powder X-ray diffraction (XRD) on a Bruker D8 Advance Da Vinci diffractometer. Optical properties were probed by diffuse reflectance UV-Vis spectroscopy (DRUVS) using a Shimadzu UV-2450 spectrophotometer. X-ray photoelectron spectra were acquired on a Kratos HSi spectrometer equipped with a charge neutralizer and monochromated Al K_α excitation source (1486.7 eV). Binding energies were referenced to adventitious carbon at 284.6 eV. Spectral fitting was performed using a common asymmetric peak shape. Errors were estimated by varying the Shirley background-subtraction procedure across reasonable limits and re-calculating the components fits. Fluorescence Pt L_{III}-edge X-ray absorption spectra (XAS) were acquired with a Lytle detector on the BL14W1 beamline of the Shanghai Synchrotron Radiation Facility (SSRF), Shanghai Institute of Applied Physics (SINAP), China, operated at 3.5 GeV with injection currents of 140–210 mA. Brunauer–Emmett–Teller (BET) surface areas were measured using a TriStar II 3020 Micromeritics porosimeter via nitrogen physisorption at 77 K. Transmission electron microscopy (TEM), high angle annular dark field scanning transmission electron microscopy (HAADF)-STEM and elemental mapping was performed on a FEI Talos F200X microscope operated at 200 kV. Particle size distributions were determined from analysis of 200 particles for all samples.

Catalytic testing

Photocatalytic water splitting was conducted in the Pyrex topped reaction cell employing 50 mg of Pt/TiO₂ catalyst dispersed in 80 mL water and 20 mL methanol at 25 °C, equilibrated in the dark for 30 min. The reaction cell was subsequently evacuated and irradiated by a 300 W Xe lamp to provide an approximate flux inside the reaction vessel of 130 mW/cm². Evolved gases in the reactor headspace were analyzed by gas chromatography (GC-9200 equipped with TCD, employing a 6 m x 2 mm x 250 µm MS-5A column). Evolved oxygen was not detected in any experiment, even using pure water in the absence of methanol as a hole scavenger, consistent with literature for PtTiO₂(anatase) [9]. Note that the parent anatase evolved ~55 µmol/h of hydrogen in the absence of platinum.

Acknowledgements

We thank the National Key R&D Program of China(2016YFC0207103), Shanghai Natural Science Foundation (14ZR1421900), National Science Foundation of China (50906050) and EPSRC (EP/K021796/1 and EP/K029525/2) for financial support.

Keywords: Platinum • TiO₂ • co-catalyst • water splitting • XPS

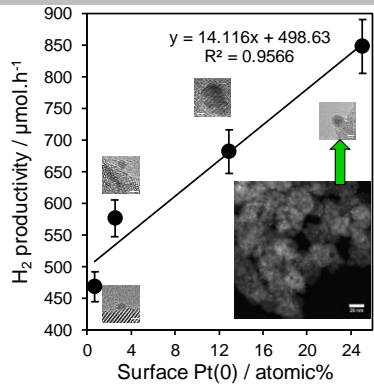
- [1] A. Fujishima, *Nature* **1972**, *238*, 37-38.
- [2] a) J. Cai, M. Wu, Y. Wang, H. Zhang, M. Meng, Y. Tian, X. Li, J. Zhang, L. Zheng, J. Gong, *Chem* **2017**, *2*, 877-892; b) J. Cai, Y. Wang, Y. Zhu, M. Wu, H. Zhang, X. Li, Z. Jiang, M. Meng, *ACS applied materials & interfaces*

- 2015, 7, 24987-24992; c) Y. Wang, J. Cai, M. Wu, H. Zhang, M. Meng, Y. Tian, T. Ding, J. Gong, Z. Jiang, X. Li, *ACS applied materials & interfaces* **2016**, 8, 23006-23014; d) M. Ni, M. K. Leung, D. Y. Leung, K. Sumathy, *Renewable and Sustainable Energy Reviews* **2007**, 11, 401-425.
- [3] a) X. Chen, S. Shen, L. Guo, S. S. Mao, *Chem. Rev.* **2010**, 110, 6503-6570; b) K. Maeda, K. Domen, *J. Phys. Chem. Lett.* **2010**, 1, 2655-2661; c) R. Abe, J. *Photochem. Photobiol. C* **2010**, 11, 179-209; d) J. Yang, D. Wang, H. Han, C. Li, *Acc. Chem. Res.* **2013**, 46, 1900-1909; e) A. Kudo, *Catal. Surv. Asia* **2003**, 7, 31-38; f) J. S. Lee, *Catal. Surv. Asia* **2005**, 9, 217-227; g) J.-M. Herrmann, *Catal. Today* **1999**, 53, 115-129.
- [4] a) S. K. Parayil, H. S. Kibombo, C.-M. Wu, R. Peng, T. Kindle, S. Mishra, S. P. Ahrenkiel, J. Baltrusaitis, N. M. Dimitrijevic, T. Rajh, *J. Phys. Chem. C* **2013**, 117, 16850-16862; b) C.-H. Lin, J.-H. Chao, C.-H. Liu, J.-C. Chang, F.-C. Wang, *Langmuir* **2008**, 24, 9907-9915; c) R. Navarro, J. Arenales, F. Vaquero, I. González, J. Fierro, *Catal. Today* **2013**, 210, 33-38; d) X. Jiang, X. Fu, L. Zhang, S. Meng, S. Chen, *J. Mater. Chem.* **2015**, 3, 2271-2282.
- [5] Y. H. Li, J. Xing, Z. J. Chen, Z. Li, F. Tian, L. R. Zheng, H. F. Wang, P. Hu, H. J. Zhao, H. G. Yang, *Nat. Commun.* **2013**, 4, 2500.
- [6] J. Xing, J. F. Chen, Y. H. Li, W. T. Yuan, Y. Zhou, L. R. Zheng, H. F. Wang, P. Hu, Y. Wang, H. J. Zhao, Y. Wang, H. G. Yang, *Chem. Eur. J.* **2014**, 20, 2138-2144.
- [7] Z. Jiang, Z. Zhang, W. Shangguan, M. A. Isaacs, L. J. Durndell, C. M. A. Parlett, A. F. Lee, *Catal. Sci. Tech.* **2016**, 6, 81-88.
- [8] a) Z. Jiang, H. Guo, Z. Jiang, G. Chen, L. Xia, W. Shangguan, X. Wu, *Chem. Commun.* **2012**, 48, 9598-9600; b) Z. Jiang, W. Shangguan, *Catal. Today* **2015**, 242, 372-380.
- [9] R. Li, Y. Weng, X. Zhou, X. Wang, Y. Mi, R. Chong, H. Han, C. Li, *Energy Environ. Sci.* **2015**, 8, 2377-2382.
- [10] R. J. Joseyphus, T. Matsumoto, H. Takahashi, D. Kodama, K. Tohji, B. Jeyadevan, *Journal of Solid State Chemistry* **2007**, 180, 3008-3018.
- [11] a) L. K. Ono, B. Yuan, H. Heinrich, B. R. Cuenya, *J. Phys. Chem. C* **2010**, 114, 22119-22133; b) F. Pesty, H.-P. Steinrück, T. E. Madey, *Surf. Sci.* **1995**, 339, 83-95.
- [12] J. Zhang, M. Zhang, Z. Jin, J. Wang, Z. Zhang, *Appl. Surf. Sci.* **2012**, 258, 3991-3999.
- [13] A. I. Frenkel, C. W. Hills, R. G. Nuzzo, *J. Phys. Chem. B* **2001**, 105, 12689-12703.

Entry for the Table of Contents

FULL PAPER

Pt metal is the active co-catalyst in photocatalytic H₂ production over anatase titania



Zhi Jiang,^{*[a]} Mark A. Isaacs,^[b] Wenfeng Shangguan,^[a] Yifeng Deng,^[c] and Adam F. Lee^{*[b]}

Page No. – Page No.

Rational design of Pt co-catalysts for photocatalytic hydrogen production over titania